Atomistic Origin of Kinetics in Hydrated Aluminosilicate Gels upon Precipitation

Cheng Zhao[1,2], Jiahui Yu[1,2], Xuyong Chen[1,2], Qiaoyun Wu[1,2,a)],
Wei Zhou[3,b)], Mathieu Bauchy[4,c)]

[1] School of Civil Engineering and Architecture, Wuhan Institute of Technology, Wuhan 430074, China
[2] Hubei Provincial Engineering Research Center for Green Civil Engineering Materials and Structures, Wuhan 430074, China
[3] State Key Laboratory of Water Resources and Hydropower Engineering Science, Wuhan University, Wuhan 430072, China
[4] Physics of AmoRphous and Inorganic Solids Laboratory (PARISlab), Department of Civil and Environmental Engineering, University of California, Los Angeles California 90095, U.S.A.

[a)]Author to whom correspondence should be addressed: wuqiaoyun@wit.edu.cn
[b)]Author to whom correspondence should be addressed: zw_mxx@whu.edu.cn
[c)]Author to whom correspondence should be addressed: bauchy@ucla.edu

Abstract

Calcium–alumino–silicate–hydrate ($CaO–Al_2O_3–SiO_2–H_2O$, or C–A–S–H) gel, which is the binding phase of cement-based materials, greatly influences concrete mechanical properties and durability. However, the atomic-scale kinetics of the aluminosilicate network condensation remains puzzling. Here, based on reactive molecular dynamics simulations (ReaxFF) of C–A–S–H systems formation with varying Al/Ca molar ratios, we study the kinetic mechanism of the hydrated aluminosilicate gels upon precipitation. We show that the condensation activation energy decreases with the Al/Ca molar ratio, which suggests that the concentration of the Al polytopes has a great effect on controlling the kinetics of the gelation reaction. Significantly, we demonstrate that 5-fold Al atoms are mainly forming at high Al/Ca molar ratios since there are insufficient hydrogen cations or extra calcium cations to compensate the negatively charged Al polytopes at high Al/Ca molar ratios during accelerated aging.

Keywords: Calcium–Alumino–Silicate–Hydrate Gel, Gelation, Kinetics, Activation energy

1. Introduction

Concrete is a complex cement-based material that is commonly utilized in human lives. Cement is the source of concrete strength as a binding component, and its micro-structure determines the mechanical properties and durability of concrete. However, cement manufacturing emits a significant amount of carbon dioxide, with around 0.75 tons of carbon dioxide emission per ton of cement [1-4]. To this end, numerous research-

ers have attempted to use green supplementary cementitious materials (SCMs) to partially replace some cement in order to reduce the carbon emission footprint of ordinary Portland cement [5-7]. Blast furnace slag and fly ash, both industrial wastes, are the most widely used SCMs due to their low cost and availability [5, 8, 9]. Generally speaking, calcium–silicate–hydrate (C–S–H) is the main hydration product of ordinary Portland cement (OPC) and the main binding phase of cement-based materials. When OPC is mixed with blast furnace slag and fly ash, the new reaction product is calcium–alumino–silicate–hydrate (C–A–S–H) gel phase. Due to the presence of aluminum oxides, this gel phase plays a significant role in the structure, mechanical properties and durability of cement-based materials[10,11]. Better understanding the formation of C–A–S-H gels can provide us with guidance to develop novel concrete materials featuring desirable performances and achieving low carbon footprints[12, 13].

In general, the process of C–A–S–H gel formation can be attributed to the dissolution-precipitation process [14-17]. When cement, slag, or fly ash are dissolved in water, the solution concentration of silicon, aluminum, and calcium ions increases[14]. The solution eventually becomes supersaturated, and the C–A–S–H gel begins to precipitate[17]. This precipitation process is directly impacted by its kinetic properties. In recent decades, many researchers have widely attempted to investigate the precipitation kinetics of C–A–S–H gels by means of laboratory experiments [18-21]. For example, Zhang *et al.* found that when the alkalinity of the solution increases, it's easier to precipitate silicon and aluminum atoms, thus favoring the formation of C–A–S–H gels [21]. Nevertheless, it is challenging to explore the kinetic mechanism for the early-age precipitation of C–A–S–H gel through experiments due to the swiftness of the reaction stage and the heterogeneous nature of the gel structure [22-25]. Meanwhile, since the C–A–S–H formation contains a succession of chemical reactions, understanding the insights into C–A–S–H gels polymerization at the nano-scale is critical to providing a fundamental reference for analyzing how aluminum influences the early-age polymerization of such gels. Therefore, the kinetic properties of C–A–S–H precipitation at the nanoscale remain unclear. Especially, the atomistic origin of its chemical composition is still poorly understood.

Compared with physical experiments, atomic-level molecular dynamics simulations give useful insights into the kinetics of C–A–S–H gelation process and provide an alternative method to conventional experiments, making it possible to study the evolving gel structures with time at the nanoscale [16, 26]. It is reported that a C–A–S–H gel has an amorphous structure comparable to a C–S–H gel, which is usually defined as a tobermorite-like but mostly cross-linked structure in molecular dynamics simulations [27, 28]. Since the structure of such gel upon precipitation is time-evolving, the atomic simulation of its early-age polymerization remains a challenge. Fortunately, the occurrence and development of Reactive Force Field (ReaxFF) provides a convenient way to simulate chemical reactions in the system with comparable accuracy to first-principles methods but with less time required [29-32]. As such, several studies have recently used reactive molecular dynamics simulation to properly describe the chemical reactivity of hydrated silicate phases [5, 16, 17].

Here, we use reactive molecular dynamics simulations to reveal the kinetic mechanism

of hydrated aluminosilicate gels upon precipitation. We first investigate the structural evolution of the C–A–S–H gel during gelation at different reaction temperatures. Based on these predictions, we further explore the effects of the Al/Ca molar ratio on reaction activation energy and polymerization reaction rate, which are compared to available experimental data. As a major outcome of this work, we demonstrate that the concentration of the Al polytopes significantly affects the kinetics of the polymerization reaction. Importantly, we show that 5-fold coordinated Al atoms are forming at high Al/Ca molar ratios but not at low Al/Ca molar ratios because there aren't enough Ca cations to compensate the negatively charged Al polytopes at high Al/Ca molar ratios during accelerated aging.

2. Methods

2.1 ReaxFF potential

The reactive ReaxFF forcefield is a bond order-based potential, and it is capable of describing bonds formation and breakage dynamics based on interatomic bond orders which depend on each atom's local environment [32]. Unlike classical potentials that depend on fixed charges, the ReaxFF potential can dynamically assign the charges of atoms via an implemented charge equilibration (QEq) means, which is critical for modeling chemical reactivity [33]. The total energy of the ReaxFF system consists of ten different energies, namely, Coulomb potential energy, van der Waals energy, under-coordination energy, long-range electron pairs energy, over-coordination energy, torsion energy, short-range bond energy, conjugation energy, penalty energy, and valence angle energy [17, 29]. More detailed information about these items can be found in Refs. [29] and Refs. [34]. Recently, the ReaxFF potential has been shown to provide a realistic description of disordered materials and their interaction with water, such as hydrated cementitious material [5, 16, 17]. Here, using the ReaxFF potential parameterized by Pitman *et al.* [32], we can simulate the kinetics of C–A–S–H gel upon precipitation. More information about the full interatomic potential parameters is available in the Supplemental Material. Note that the parametrization of ReaxFF used here has already been extensively studied and validated for various hydrated silicate systems e.g., C–S–H gel, C–A–S–H gel [9, 16, 17, 25, 35]. All the simulations are performed with the USER-REAXC implementation of ReaxFF, which is included in the large-scale atomic/molecular massively parallel simulation (LAMMPS) package[34] . The velocity-Verlet integration algorithm with a timestep of 0.25 fs is employed to numerically calculate the motion of the atoms.

2.2 Simulation details

Here, we prepare a series of hydrated aluminosilicate gels with the chemical formula $(CaO)_{1.7}(Al_2O_3)_x(SiO_2)_{1-x}(H_2O)_{3.7+x}$, where x (the amount in moles of Al_2O_3) = 0.00, 0.02, 0.05, 0.08, 0.10, 0.12, 0.15, 0.17, 0.19, 0.22, and 0.26 [35]. The corresponding Al/Ca molar ratios are 0.00, 0.03, 0.06, 0.09, 0.12, 0.14, 0.17, 0.20, 0.22, 0.26, and 0.30, respectively. It should be noted that the composition formula of C–A–S–H gel is defined here based on the molar ratio of any two compounds rather than the concentration to directly represent the role of aluminum oxides when added to ordinary cements. For example, the $CaO/(Al_2O_3 + SiO_2)$ molar ratio is kept fixed at 1.7, which corresponds to the average stoichiometry of the C–A–S–H gel forming upon the hydration of ordinary

Portland cement [16,17]. These selected compositions are consistent with typical stoichiometries of slag-based cements observed in the laboratory [16, 17, 35, 36]. All simulated systems comprise about 4000 atoms, and the detailed composition and size of these eleven C–A–S–H systems can be found in Ref. [35]. The precipitation of a C–A–S–H gel is modeled by adopting the methodology proposed by Côté and Cormack et al. [37], which has been extensively used to investigate the binding phase of cement-based materials[16, 17 35].

In the beginning, we utilize the PACKMOL package [38] to generate the initial configuration by randomly putting isolated $Ca(OH)_2$, $Al(OH)_3$, and $Si(OH)_4$ molecules into a cubic simulation box with a length of 40 Å. All molecules are guaranteed to prevent any unrealistic overlap, and periodic boundary conditions are applied in the cubic box. Subsequently, the initial configuration is relaxed for 100 ps in a canonical (*NVT*) ensemble at 300 K by using the Nosé-Hoover thermostat [39, 40]. The obtained system is then relaxed for 500 ps in an isothermal-isobaric (*NPT*) ensemble under 0 atm of pressure and 300 K [16]. The duration of this relaxation stage is long enough to achieve the convergence of both volume and energy in the initial system. An example of the atomic snapshot of the simulated C–A–S–H gel after the initial relaxation at 300 K is shown in **Fig. 1(a)**. As the energy barriers of the condensation reaction are too large to be overcome within the finite time scale of reactive molecular dynamical simulation at 300 K, we do not observe any formation of Si–O–Si, Al–O–Al, or Si–O–Al linkages in this configuration. Finally, to speed up the gelation dynamics, the initial relaxed system is exposed to an accelerated aging process that heats the system to a high temperature (varying from 1500 to 3000 K) for 1.25 ns in the *NVT* ensemble. Such accelerated aging technique is widely employed to accelerate the condensation reaction in reactive molecular dynamical simulations [17, 41]. In detail, the energy barrier associated with the breaking of Si–O–H, Al–O–H bonds and subsequent formation of Si–O–Si, Si–O–Al and Al–O–Al bonds is about 96 kJ/mol [16,26]. For this system, the thermal energy (*NkT*) with a temperature *T* in the range of 1500 to 3000 K is about 1325e-20 ~ 2650e-20 kJ, which is close to the total condensation energy barrier (about 3142e-20 kJ). Therefore, at this stage, these aluminate and silicate monomers gradually condensate and generate some aluminosilicate chains/rings [see **Fig. 1(b)**]. In addition, all molecular dynamics simulations are repeated six times for statistical averaging. The simulated results are the average of six repeated calculations, and the error bars are determined from the standard deviation of the six simulations.

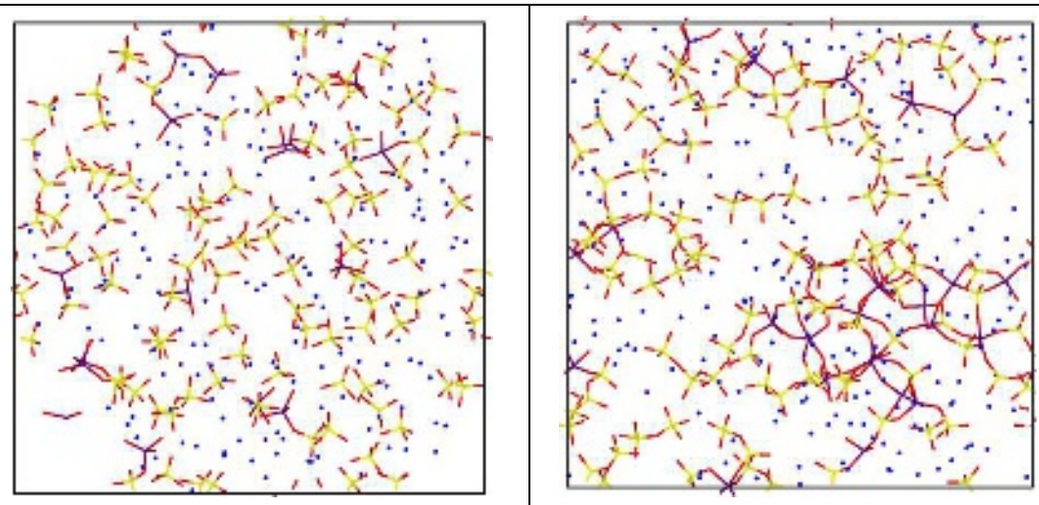

(a) t = 0.00 ns | **(b)** t = 1.25 ns

Fig. 1. Atomic snapshots presenting the simulated configurations of a $CaO–Al_2O_3–SiO_2–H_2O$ (C–A–S–H) gel with Al/Ca = 0.09 **(a)** after the first relaxation at 300 K and before accelerated aging, and **(b)** after 1.25 ns of reaction at an elevated temperature (e.g. 2000 K). Note that, only the Ca atoms, and bonds of Al–O and Si–O are shown for clarity. Al, Ca, Si, and O atoms are displayed in purple, blue, yellow, and red, respectively.

2.3 Structure analysis

In order to describe the kinetics of the precipitation of C–A–S–H systems, we focus on how the atomic structure and topology of the C–A–S–H gels upon gelation evolve over time. Especially, more attention is paid to the oxygen (O) atoms' local environment to capture the degree of polymerization of the network. To this end, it's first necessary to compute the partial pair distribution functions (PDFs) of atom pairs, which are commonly used to represent the distribution of atoms in the study of molecular materials. In general, the partial pair distribution function $g(r)$ can be defined as the probability distribution of other atoms on the coordination spherical shell with a radius of *r* centered on atom *i*. In detail, $\rho(r)$ is defined as the average local number density of atoms at a distance *r*, and the average number of atoms $n(r)$ in a coordination spherical shell can be defined as follows [41]:

$$n(r) = \int_r^{r+dr} 4\pi r^2 \rho(r) dr \tag{1}$$

correspondingly, the number of atoms specified on the coordination spherical shell layer of thickness dr can be evaluated as follows [41]:

$$dn(r) = 4\pi r^2 \rho(r) dr \tag{2}$$

where $\rho(r) = \rho_0 g(r)$ and ρ_0 is the bulk density of atoms. Therefore, the pair distribution function $g(r)$ may be calculated by the following formula [41]:

$$g(r) = dn(r)/(\rho_0 * 4\pi r^2 dr) \tag{3}$$

Note that the PDFs can be compared to the experimental results of X-ray or neutron diffraction of materials. The partial PDFs of Al−O, Si−O, Ca−O, H−O, Al−H, and Al−Ca pairs can be found in **Fig. S1** and **Fig. S2** in Supplemental Material. Secondly, the posi-

tion of the minimum after the first peak in the partial pair distribution function is defined as the cut-off point to distinguish the first and second coordination shells. The obtained cutoffs in this work for Si–O, Al–O, and H–O bonds are 2.2 Å, 2.0 Å, and 1.2 Å, respectively. Lastly, the partial coordination number of each atom is computed by enumerating neighboring atoms' numbers in the first coordination shell [4]. According to their partial coordination numbers, the O atoms in the C–A–S–H gel can be divided into bridging oxygen (BO) atoms that are linked to two skeleton atoms (Si or Al) and non-bridging oxygen (NBO) atoms that are linked to one skeleton atom. The evolution of the fraction of BO atoms is typically taken as an index to quantify the total degree of polymerization (i.e., network connectivity).

3. Results and Discussion

3.1 Effect of temperature

We first assess the effect of temperature on the kinetics of the gelation of C–A–S–H gels. For this purpose, the evolutions of the BO/(Si + Al) molar ratio as a function of time during accelerated aging at various temperatures (i.e., 1500 K, 2000 K, 2250 K, 2500 K, and 3000 K) are calculated for the eleven compositions. On the contrary, higher temperatures cause the system to melt, which greatly affects the gelation mechanism. **Fig. 2** shows the evolutions of the number of bridging oxygens (i.e., Si–O–Si, Si–O–Al, and Al–O–Al) atoms per Si and Al atoms [BO/(Si + Al)] in the simulated C–A–S–H system with Al/Ca = 0.06 and (b) Al/Ca = 0.30 during accelerated aging at select reaction temperatures. On the one hand, for each composition (see **Fig. S5** in **Supplemental Material**), we observe that the overall polymerization degree (BO/(Si + Al) molar ratio) of the C–A–S–H system gradually increases as the precipitation proceeds and ultimately gets to a plateau, which is similar to recent findings that the degree of polymerization of C–S–H was also found to gradually increases over time and eventually reaches a plateau in the case of the gelation of Al-free C–S–H gels [16].On the other hand, we note that the polymerization rate rises with an increase in temperature, and higher temperatures could lead to quicker kinetics of the condensation reaction. Nevertheless, the ultimate value of the BO/(Si + Al) molar ratio for each composition is unaffected by the reaction temperature. This also demonstrates that the gelation kinetics can be enhanced by such high temperatures while having no effect on the ultimate configuration of the gel [16, 26].

In order to quantitatively evaluate the temperature-dependence of the gelation kinetics, the reaction polymerization rate k for each temperature is determined by fitting the BO/(S i+ Al)(t) curve shown in **Fig. 2** with a first-order exponential relaxation function as follows[16]:

$$\mathrm{BO/(Si+Al)}(t) = A[1 - \exp(-kt)] \tag{4}$$

where A is the final value of the BO/(Si+Al) molar ratio at infinite time t. **Fig. 3(a)** shows the evolutions of polymerization rate of C–A–S–H gels during accelerated aging at 2000 K as a function of the initial Al/Ca molar ratio, with the gray area representing the slop variation. It can be observed that the polymerization rate at 2000 K increases significantly as the Al/Ca molar ratio increases, which indicates that the addition of $Al(OH)_3$ monomers can significantly accelerate the kinetics of the gelation reaction. Furthermore, we compute the polymerization rates at these reaction temperatures for

various compositions based on Eq.(3). As shown in **Fig. 3(b)**, the obtained polymerization rate values reflect an Arrhenius-like dependence on temperature.

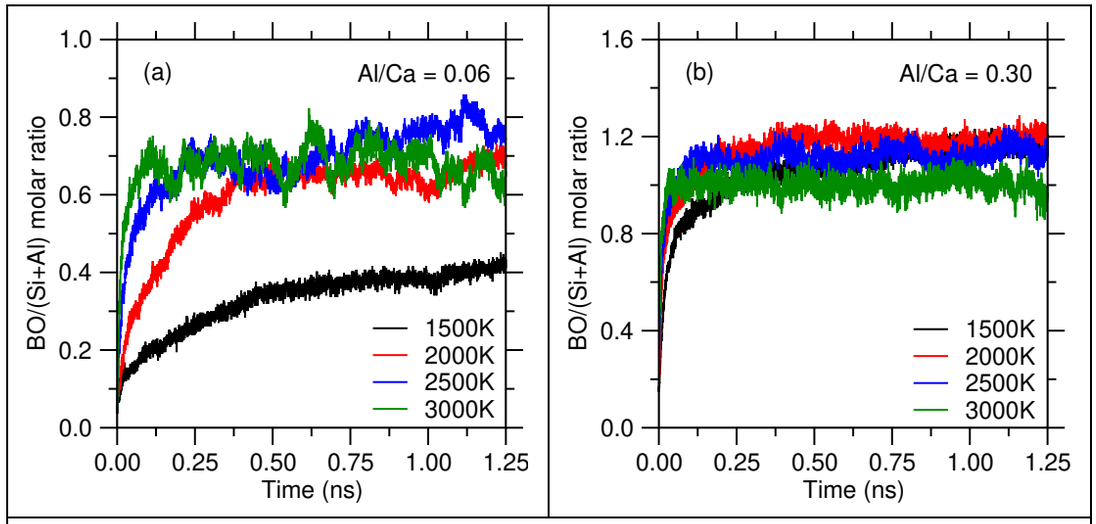

Fig. 2. Evolutions of the number of bridging oxygens (i.e., Si–O–Si, Si–O–Al, and Al–O–Al) atoms per Si and Al atoms [BO/(Si + Al)] in the simulated C–A–S–H system with **(a)** Al/Ca = 0.06 and **(b)** Al/Ca = 0.30 during accelerated aging at select reaction temperatures.

3.2 Activation energy of gelation reaction

We now calculate the activation energy of the gelation reaction to deeply investigate the temperature-dependence of the kinetic process. Generally, the activation energy of condensation E_a can be determined by fitting the reaction temperature and polymerization rate [see **Fig. 3(b)**], with the Arrhenius equation as follows [42]:

$$k(T) = k_0 \exp\left(-E_a/RT\right) \tag{5}$$

where T is the temperature, k_0 is the polymerization rate at infinite temperature, and R is the perfect gas constant. **Fig. 3(c)** shows the evolution of the computed activation energy of C–A–S–H gelation with the Al/Ca molar ratio. For Al/Ca = 0.00, we observe the activation energy value is 114 kJ/mol, which can be compared with the previous simulation results and available experimental data (about 96 kJ/mol) [16]. At this point, the obtained total kinetic energy is about 3711 ~ 7422 kJ/mol which is greater than 100 kJ/mol. As shown in **Fig. 3(c)**, the activation energy first dramatically decreases with the increase of the Al/Ca molar ratio, and the activation energy is only 63 kJ/mol when the Al/Ca molar ratio is 0.14; then the activation energy decreases steadily as the Al/Ca molar ratio increases, eventually reaching 50 kJ/mol when the Al/Ca molar ratio is 0.30. Meanwhile, the gray area in **Fig. 3(c)** depicts when the Al/Ca molar ratio is greater than or equal to 0.14, the decreasing rate of the activation energy reduces. This indicates that aluminum atoms in solution lower the magnitude of the energy barrier associated with gelation reaction, but once the amount of aluminum reaches a certain level or saturation, the reduction in the energy barrier decreases considerably.

The possible reasons for this phenomenon are grouped into two facts. On the one

hand, when the concentration of aluminum cation in solution is low and calcium cation is moderate, calcium atoms act as catalysts during the gelation process and accelerate the kinetics of precipitation of C–A–S–H gels, which is consistent with prior studies [41, 43]. Moreover, calcium atoms tend to cause nano-segregation within the gel to favor the generation of calcium-rich and aluminosilicate-rich regions [5,44]. Such nanosegregation reduces the moving area of $Si(OH)_4$ and $Al(OH)_3$ monomers and brings monomers and oligomers closer, increasing the collision probability between them and eventually improving the polymerization rate [5,16]. On the other hand, when the concentration of aluminum cation in the aqueous solution increases to a certain point but the concentration of calcium decreases, the calcium atoms continue to act as catalysts. At this point, the high concentration of aluminum cation causes some nanoscale phase separation, wherein Si and Al species are largely segregated into different regions [35]. Because silicon and aluminum atoms are both network-forming atoms, the kinetic mechanism of phase separation between them is different from the nano-segregation of the formation of calcium-rich and silicon-aluminum-rich regions. In other words, this nanoscale phase separation not only makes $Al(OH)_3$ monomers and oligomers (containing Al atoms) closer, but also brings $Si(OH)_4$ monomers and oligomers (containing Si atoms) closer, thereby enhancing the collision probability among them and accelerating the formation rate of silicon and aluminum polymers in the polymerization reaction to some extent. However, because the energy barriers required to form aluminosilicate polymers are lower than those required to form silicon and aluminum polymers alone, the activation energy of the polymerization reaction continues to decline at this time, albeit at a slower rate.

In turn, the polymerization rate of C–A–S–H gel at 300 K can be estimated from Eq. (3). As depicted in **Fig. 3(d)**, the polymerization rate at 300 K begins to increase significantly when Al/Ca = 0.14, which coincides with the observed change in the trend of the reaction activation energy. The maximum polymerization rate at 300 K reaches a value of about 1300 s^{-1} when Al/Ca = 0.30. It is worth noting that the accuracy of the predicted polymerization rate directly depends on the quality of the data fitting [see **Fig. 3(b)**]. Nonetheless, the overall trend of the evolution of the polymerization rate at 300 K is unaffected by this uncertainty, which is consistent with the trend of the polymerization rate at 2000 K [see **Fig. 3(a)**]. These simulation results suggest that the addition of aluminum atoms may greatly raise the polymerization rate of the C–A–S–H gel.

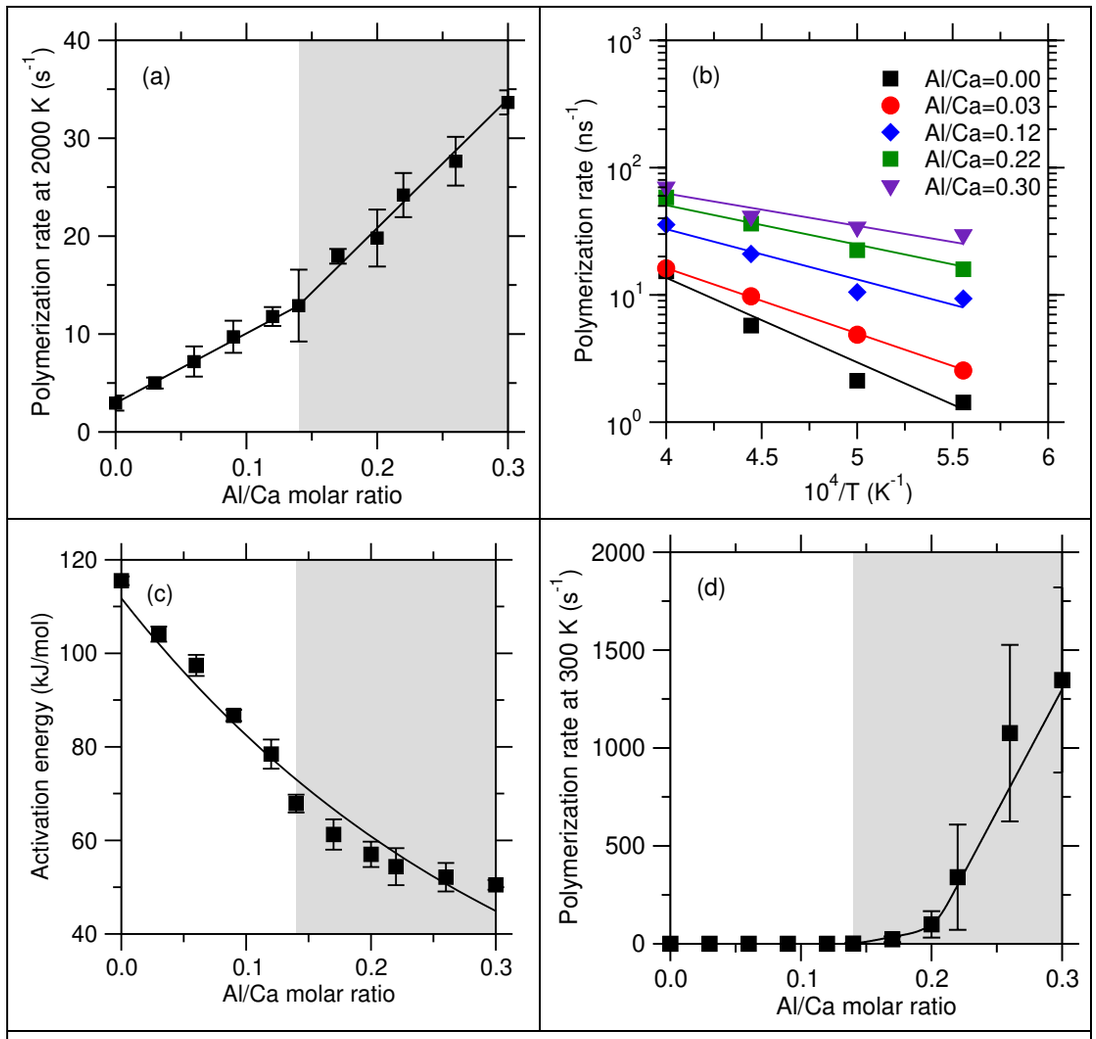

Fig. 3. (a) Polymerization rate at 2000 K as a function of the Al/Ca molar ratio. **(b)** Arrhenius representation of the temperature-dependence of the initial polymerization rate of gels with several Al/Ca molar ratios. The data are fitted by the exponential relaxation function. **(c)** Activation energy of C–A–S–H gels gelation and **(d)** Polymerization rate at 300 K as a function of Al/Ca molar ratio. The lines are to guide the eye. The data are fitted by the Arrhenius equation. The grey area indicates that the break in slope in the activation energy.

3.3 Effect of Al coordination number

Next, we explore the effect of coordination number of the aluminum atom on the activation energy and the polymerization rate of C–A–S–H gelation process. Based on the partial pair distribution function of Al–O atomic pair (see **Fig. S1**), we calculated the coordination number of each aluminum atom. Note that the coordination number of aluminum atoms is not fixed in this system, so it's necessary to pay more attention to the average coordination number of aluminum atoms. Moreover, the results of the average coordination numbers for other kinds of atoms, and the mean coordination numbers related to Al−H and Al−Ca pairs in C–A–S–H gels can also be found in **Fig. S3** and **Fig. S4**. **Fig. 4(a)** presents the average coordination number of aluminum atoms in the C–A–S–H gels before accelerated aging at 2000 K as a function of the Al/Ca molar ratio. When the Al/Ca molar ratio is less than 0.14, the average coordination number

of aluminum atoms exceeds 4 and increases slowly because the low concentration of aluminum cations in the solution results in a small number of formed polymers. In contrast, when the Al/Ca molar ratio is greater than or equal to 0.14, the average coordination number of aluminum atoms also exceeds 4 but increases obviously. As expected, the breaking position (i.e., Al/Ca = 0.14) from the curve slope of mean coordination number of Al atoms is found same to that in the both curves of activation energy and the polymerization reaction rate at 300K, revealed in **Figs. 3(c)** and **(d)**. This finding suggests that the growth of the average coordination number of aluminum atoms reduces the energy barrier in the gelation process and speeds up the polymerization rate of C–A–S–H gels at room temperature.

Moreover, the results of the molecular dynamics simulation show Moreover, the results of the molecular dynamics simulation show the presence of 4-fold, 5-fold, and 6-fold coordinated aluminum atoms in the system (see Fig. **S6**), which are close to the experimental results obtained from the ^{27}Al NMR (Nuclear Magnetic Resonance) test, wherein the 4-fold (with a fraction of about 75%), 5-fold (with a fraction of about 10%), and 6-fold (with a faction of about 15%) coordinated aluminums are observed on C–A–S–H samples with low Ca/Si molar ratio [45]. The fraction of 5-fold Al atoms in hydrated aluminosilicate gels with the Al/Ca molar ratio before accelerated aging at 2000 K exhibits a change trend that is significantly related to kinetic properties, as illustrated in **Fig. 4(b)**. It is clear that the fraction of 5-fold Al atoms gradually increases with the increasing Al/Ca molar ratio. When Al/Ca molar ratio is larger than 0.14, the increasing rate of 5-fold Al atoms abruptly changes, and the fraction of 5-fold Al atoms reaches up to 6%, which is much greater than the case where the Al/Ca molar ratio is less than 0.14. This finding is consistent with the previous change in activation energy and polymerization rate at 300 K, which directly indicates that the existence of 5-fold Al atoms accelerates the precipitation kinetics of C–A–S–H gel. In fact, from an experimental point of view, 5-fold Al atoms easily result in the formation of so-called coordinatively unsaturated sites (CUS), which are present on the surface or in surface near areas and are thought to have high Lewis acidity [46-48]. As a result, the polymerization rate is enhanced, implying that 5-fold Al atoms act as potential catalysts, which is in agreement with earlier experimental findings [49, 50]. That is to say, the presence and addition of 5-fold Al atoms before accelerated aging at 2000 K requires more cations (e.g., H^+ or Ca^{2+}) for charge compensating, which, in turn, may lead to an increase in the pH value of the solution, thus accelerating the polymerization kinetics. Overall, our findings support the idea that the coordination number of aluminum in C–A–S–H gel plays a key role in affecting the gelation kinetics.

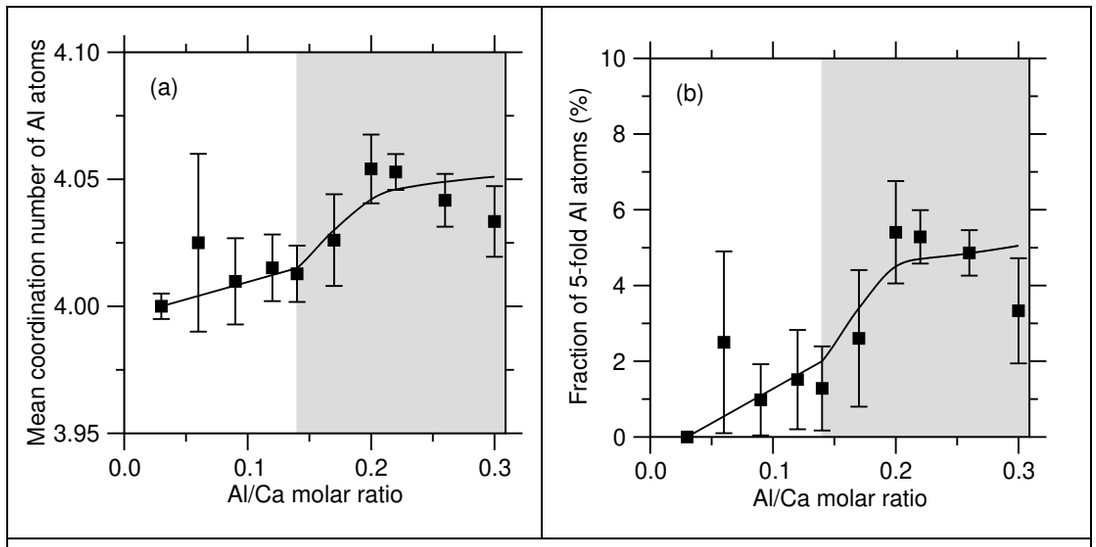

Fig. 4. (a) Mean coordination number of Al atoms and **(b)** fraction of 5-fold coordinated Al atoms in hydrated aluminosilicate gels as a function of Al/Ca molar ratio before accelerated aging at 2000 K. The lines are to guide to the eye. The grey area indicates that the break in slope.

3.4 Mechanism of charge compensation

Finally, we further focus on the reasons for the increase of 5-fold coordinated Al atoms in the C–A–S–H gels with the Al/Ca molar ratio before accelerated aging at 2000 K. To this end, we investigate the effect of the charge compensation mechanism on the kinetics of the precipitation of C–A–S–H gels by computing the charges of various atoms in the present systems. Generally speaking, the oxygen atoms before the gelation reaction may be divided into NBO atoms and free oxygen (FO) atoms according to the topology. The FO atoms are the oxygen atoms that are neither connected to silicon atoms nor aluminum atoms. These oxygen atoms include the oxygen atoms typically balanced in charge with calcium cations and hydrogen cations, and the isolated oxygen atoms (the proportion in this work is almost zero). Due to the variable number of aluminum atoms, it's easy to form negatively charged AlO_4^{1-}, AlO_5^{2-} , and AlO_6^{3-} aluminum polytopes when the Al concentration increases (see **Fig. S7**), which is consistent with the previous finding in silicate glasses [51]. These negatively charged aluminum polytopes require hydrogen cations with one positive charge or calcium cations with two positive charges for charge compensation in the C–A–S–H gels. Therefore, both hydrogen atoms and calcium atoms can be classified into the following three categories based on their specific roles: for creating NBO atoms, for forming FO atoms, and for charge balancing aluminum-oxygen polyhedra. Note that, in silicate glasses with both Na and Ca charge compensators, it is well known that negatively charged aluminum polytopes are first compensated by Na^+ ions. Depending on Al concentration, AlO_4^{1-} AlO_5^{2-} , and AlO_6^{3-} aluminum polytopes can appear where Ca ions begin to charge compensate these aluminum polytopes (per-aluminum or per-alkali glasses) [52, 53]. In addition, based on the multiple quantum (MQ) ^{27}Al NMR test, Faucon et al. proposed that AlO_4^{1-} aluminum polytopes are charge balanced predominantly by hydrogen cations in C–A–S–H gels [54]. Here, it is assumed that H^+ ions could play a similar role as Na^+ ions before Ca^{2+} ions bring their charges and increase the formation of AlO_5^{2-} and/or AlO_6^{3} aluminum polytopes. Thus, the numbers of hydrogen and calcium atoms, respectively,

required for charge balancing are N_{ComH} and N_{ComCa} , which can be calculated as follows:

$$N_{\mathrm{ComH}} = N_{\mathrm{AlO}_4^{1-}} \tag{6}$$

$$N_{\mathrm{ComCa}} = \frac{1}{2}(N_{\mathrm{AlO}_4^{1-}} - N_{\mathrm{ComH}}) + N_{\mathrm{AlO}_5^{2-}} + \frac{3}{2}N_{\mathrm{AlO}_6^{3-}} \tag{7}$$

where $N_{\mathrm{AlO}_4^{1-}}$ is the number of AlO_4^{1-} polytope, $N_{\mathrm{AlO}_5^{2-}}$ is the number of AlO_5^{2-} polytope, $N_{\mathrm{AlO}_6^{3-}}$ is the number of AlO_6^{3-} polytope. However, the real number of hydrogen and calcium atoms, respectively, available for charge compensation are N'_{ComH} and N'_{ComCa}, which can be calculated as follows:

$$N_{\mathrm{ComH}}{}' = N_{\mathrm{TotalH}} - (N_{\mathrm{NBOH}} + N_{\mathrm{FOH}}) \tag{8}$$

$$N_{\mathrm{ComCa}}{}' = N_{\mathrm{TotalCa}} - (N_{\mathrm{NBOCa}} + N_{\mathrm{FOCa}}) \tag{9}$$

where N_{TotalH} and N_{TotalCa} are, respectively, the total number of hydrogen and calcium atoms in the system; N_{NBOH} and N_{NBOCa} are, respectively, the number of hydrogen and calcium atoms used to create NBO atoms; N_{FOH} and N_{FOCa} are, respectively, the number of hydrogen and calcium atoms used to form FO atoms. Note that the total number of calcium atoms in these gels with different Al/Ca molar ratios is a constant value of 386. As the Al/Ca molar ratio increases, the amount of aluminum atoms grows, which increases the numbers of hydrogen and calcium atoms required for charge compensation. Meanwhile, the numbers of hydrogen and calcium atoms used to create NBO atoms increases, which may result in an insufficient number of hydrogen or calcium atoms actually used for charge balancing. Therefore, the numbers of missing hydrogen atoms and missing calcium atoms, respectively, for charge balancing are N_{MissingH} and $N_{\mathrm{MissingCa}}$, which can be determined as follows:

$$N_{\mathrm{MissingH}} = N_{\mathrm{ComH}} - N_{\mathrm{ComH}}{}' \tag{10}$$

$$N_{\mathrm{MissingCa}} = N_{\mathrm{ComCa}} - N_{\mathrm{ComCa}}{}' \tag{11}$$

Figure 5(a) show the fraction of missing hydrogen atoms for charge balancing in the C–A–S–H gels as a function of the Al/Ca ratio after the initial relaxation at 300 K. As illustrated in **Fig. 5(a)**, the fraction of missing hydrogen atoms for charge balancing increases with the increasing Al/Ca molar ratio. As expected, the growing rate of the fraction of missing hydrogen atoms rises when the Al/Ca ratio is larger than 0.14, which agrees with the positions of the break in slope in the activation energy reported in **Fig. 3(c)**, the polymerization rate reported in **Fig. 3(d),** and the fraction of 5-fold coordinated Al atoms shown in **Fig. 4(b)**. In detail, when the Al/Ca molar ratio is less than 0.14, the growing fraction of missing hydrogen atoms for charge balance suggests that the number of the AlO_4^{1-} aluminum polytopes is gradually more than the real number of hydrogen atoms available for charge compensation, and the effect of the charge compensation mechanism is amplified. At this point, more positively charged atoms (e.g., hydrogen atoms or calcium atoms) need to be consumed to achieve charge balance, raising the pH value of the aqueous solution, and accelerating the gelation rate. Similarly, when the Al/Ca molar ratio is greater than or equal to 0.14, the difference between the number of AlO_4^{1-} aluminum polytopes and the real number of hydrogen atoms available for charge compensation is relatively large, resulting in a

greater shortage of hydrogen atoms used for charge compensation. Meanwhile, the impact of the mechanism of charge compensation is stronger, necessitating a greater number of positively charged atoms (e.g., hydrogen atoms). As a result, the higher the pH value of the formed solution, the faster the polymerization rate.

Based on the calculation results, we find that the fraction of missing calcium atoms for charge balancing is negative in the C–A–S–H gels, which means that there are extra calcium atoms after charge compensation with aluminum polytopes. **Figure 5(b)** shows the fraction of extra calcium atoms available for charge balancing in the C–A–S–H gels as a function of the Al/Ca ratio after the initial relaxation at 300 K. We can observe that the number of extra calcium atoms gradually increases with the increasing Al/Ca molar ratio. Especially when the Al/Ca ratio is greater than 0.14, the increasing rate of the number of extra calcium atoms grows, which is also confirmed with the positions of the break in slope in the activation energy shown in **Fig. 3(c)**, the polymerization rate represented in **Fig. 3(d)**. This finding agrees with the evolution of the 5-fold coordinated Al atoms with the increase in Al/Ca molar ratio observed in **Fig. 4(b)**. To be specific, AlO_4^{1-}aluminum polytopes cannot completely be charged by H^+ cations, Ca^{2+} cations begin to charge to compensate the excess AlO_4^{1-}aluminum polytopes, the AlO_5^{2-}or AlO_6^{3-} units gradually appear as the Al/Ca molar ratio increases. When the Al/Ca molar ratio is smaller than 0.14, the fraction of extra calcium atoms available for charge balance is a small, which indicates that the number of 5-fold Al atoms is also small. At this point, the increasing positively charged calcium atoms could lead to an increase in the pH value of the aqueous solution, which tends to accelerate the gelation kinetics[55]. On the other hand, when the Al/Ca molar ratio is larger than or equal to 0.14, the more fraction of extra calcium atoms available for charge balance, the more 5-fold Al atoms are formed. At the same time, the impact of a higher pH value of the formed solution is stronger, which results in a faster gelation kinetics rate. Therefore, the increase of Ca^{2+} cations can bring more charges and increase the formation of AlO_5^{2-} and/or AlO_6^{3-} units. Generally speaking, the mechanism of charge compensation resulting from the change in atomic coordination number greatly speeds up the precipitation kinetics.

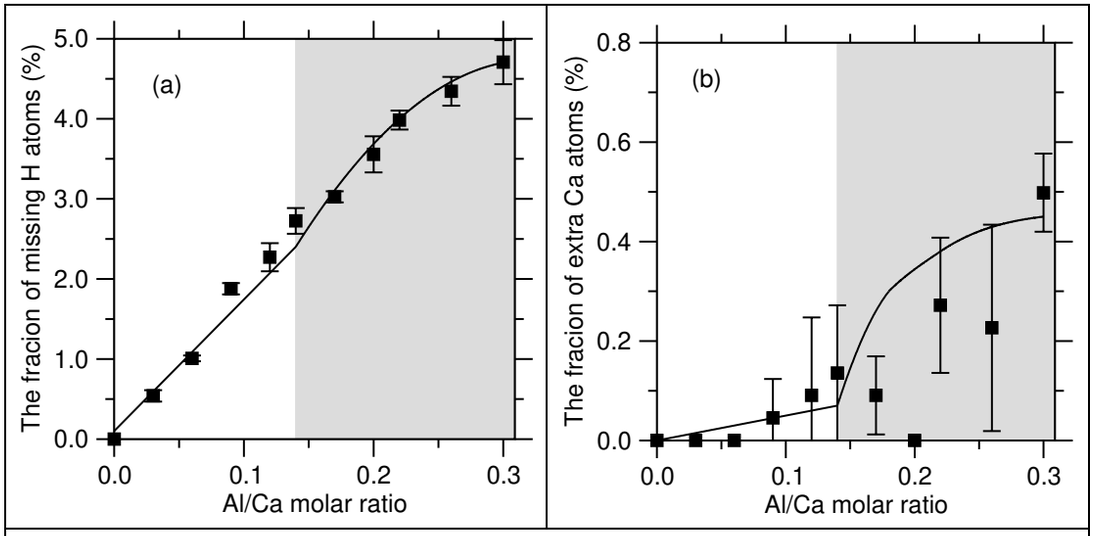

Fig. 5. The numbers of **(a)** missing H atoms and **(b)** extra Ca atoms in hydrated aluminosilicate gels with respect to the Al/Ca molar ratio before accelerated aging at 2000 K. The line is to guide to the eye. The grey area indicates that the break in slope.

4. Conclusions

Altogether, this study shows the kinetic mechanism of calcium–alumino–silicate–hydrate gel formation by reactive molecular dynamics simulations. The elevated reaction temperatures which don't affect the structure of the final hydrated gel are adopted to accelerate the condensation kinetics in the reactive molecular dynamics simulations, and the results of polymerization kinetics are in agreement with experimental data. As a major outcome of this study, we find that the condensation kinetics of the gel are strongly influenced by the concentration of Al atoms in the aqueous solution. Specifically, the activation energy of C–A–S–H precipitation decreases with the increase of the Al/Ca molar ratio, and accordingly the polymerization rate at 300K increases. Furthermore, based on the atomic coordination analysis and charge-balancing mechanism, we demonstrate that 5-fold Al atoms are mainly forming at high Al/Ca ratios, where the 5-fold Al atoms act as a potential catalyst in the gelation process. This arises from the fact that there are insufficient hydrogen atoms or extra calcium atoms to charge compensate Al atoms at high Al/Ca ratios during accelerated aging, which requires the consumption of more positively charged atoms (e.g., hydrogen atoms) for charge balancing and hence enhances the gelation rate. Overall, we envision that the careful control of the kinetics of hydrated gels could open a new avenue for designing novel gels with enhanced properties.

SUPPLEMENTARY MATERIAL

See supplementary material for the pair distribution functions of Al−O, Si−O, Ca−O, H−O, Al−H and Al−Ca pairs; the average coordination numbers of Si, Ca, H, and O atoms; the average coordination numbers related to Al−H pair and Al−Ca pairs; the evolution of the BO/(Si+Al) molar ratio as a function of time with different Al/Ca ratios; the fractions of 4-fold and 5-fold coordinated Al atoms before accelerated aging at 2000 K; the fractions of AlO_4, AlO_5 , and AlO_6 aluminum polytopes after accelerated aging at 2000 K; and the list of ReaxFF parameters used for the molecular dynamics simulations.

Acknowledgements

The authors acknowledge financial support provided by the National Natural Science Foundation of China under Grant No. 52269025, the Guizhou Provincial Science and Technology Projects under Grant No. 2023-207, the Scientific Research Project of Hubei Provincial Department of Education under Grant No. Q20221514, the Science Foundation of Wuhan Institute of Technology under Grant No. K202222, and the China Scholarship Council under Grant No. 201906270098. Part of this work was also supported by the National Science Foundation under Grants No. DMREF-1922167 and No. DMR-1944510.

AUTHOR DECLARATIONS

Conflict of Interest

The authors have no conflicts to disclose.

Author Contributions

Cheng Zhao: Conceptualization (equal); Data curation (equal); Formal analysis (equal); Investigation (equal); Writing – original draft (equal); Writing – review & editing (equal); Funding acquisition (equal). **Jiahui Yu:** Formal analysis (equal); Software (equal); Writing – review & editing (equal). **Xuyong Chen:** Investigation (equal); Writing – review & editing (equal). **Qiaoyun Wu:** Writing – review & editing (equal); Project administration (equal). **Wei Zhou:** Writing - review & editing (equal); Supervision (equal). **Mathieu Bauchy:** Methodology (equal); Funding acquisition (equal); Supervision (equal); Writing – review & editing (equal).

DATA AVAILABILITY

The data that support the findings of this study are available from the corresponding authors upon reasonable request.

References

[1] D. N. Huntzinger, and T. D. Eatmon, J. Clean. Prod. **17**,668 (2009).
[2] L. K. Turner, and F. G. Collins, Constr. Build. Mater. **43**,125 (2013).
[3] S. Tang, H. A, J. Chen, W. Yu, P. Yu, E. Chen, H. Deng, and Z. He, Appl. Surf. Sci **496**, 143744 (2019).
[4] L. Qin, X. Mao, Y. Cui, J. Bao, G. Sant, T. Chen, P. Zhang, X. Gao, and M. Bauchy, J. Chem. Phys. **157**, 234501 (2022).
[5] C. Huang, Q. Wang, C. Zhao, W. Zhou, X. Chang, X. Liu, W. Tian, and S. Zhang, J. Phys. Chem. B (2023).
[6] V. Baroghel-Bouny, K. Kinomura, M. Thiery, and S. Moscardelli, Cem. Concr. Compos. **33**,832 (2011).
[7] K. M. Rahla, R. Mateus, and L. Braganca, J. Clean. Prod. **220**,445 (2019).
[8] C. E. White, J. L. Provis, A. Llobet, T. Proffen, and J. S. J. van Deventer, J. Am. Ceram. Soc. **94**,3532 (2011).
[9] D. Hou, Z. Li, and T. Zhao, Rsc. Advances. **5**,448 (2014).
[10] S.-D. Wang, and K. L. Scrivener, Cem. Concr. Res. **25**,561 (1995).
[11] K. Ioannidou, M. Kanduc, L. Li, D. Frenkel, J. Dobnikar, and E. Del Gado, Nat. Commun. **7**, 12106 (2016).

[12] R. Hellmann, S. Cotte, E. Cadel, S. Malladi, L. S. Karlsson, S. Lozano-Perez, M. Cabie, and A. Seyeux, Nat. Mater. **14**,307 (2015).
[13] L. Wang, L. Chen, J. L. Provis, D. C. W. Tsang, and C. S. Poon, Cem. Concr. Compos. **106**, 103489 (2020).
[14] H. M. Dyson, I. G. Richardson, and A. R. Brough, J. Am. Ceram. Soc. **90**,598 (2007).
[15] K. R. Yang, and C. E. White, Langmuir **32**,11580 (2016).
[16] T. Du, H. Li, Q. Zhou, Z. Wang, G. Sant, J. V. Ryan, and M. Bauchy, Phys. Rev. Mater. **3**, 065603 (2019).
[17] C. Zhao, H. Liu, L. Guo, and M. Bauchy, J. Chem. Phys. **153**,014501 (2020).
[18] J. Yarwood, R. Douthwaite, and S. Duckett, *Spectroscopic Properties of Inorganic and Organometallic Compounds: Volume 40* (Royal Society of Chemistry, 2009).
[19] I. G. Richardson, L. Black, J. Skibsted, and R. J. Kirkpatrick, Adv. Cem. Res. **22**,233 (2010).
[20] J. L. Provis, A. Palomo, and C. Shi, Cem. Concr. Res. **78**,110 (2015).
[21] X. Ren, *Complete Recycling and Utilization of Waste Concrete Through Geopolymerization* (The University of Arizona., 2015).
[22] S. Antiohos, and S. Tsimas, Cem. Concr. Res. **34**,769 (2004).
[23] F. Puertas, M. Palacios, H. Manzano, J. S. Dolado, A. Rico, and J. Rodríguez, J. Eur. Ceram. Soc. **31**,2043 (2011).
[24] M. B. Haha, B. Lothenbach, G. L. Saout, and F. Winnefeld, Cem. Concr. Res. **42**,74 (2012).
[25] T. Du, H. Li, and M. Bauchy, ACS Appl. Nano Mater. **3**,2176 (2020).
[26] T. Du, H. Li, G. Sant, and M. Bauchy, J. Chem. Phys. **148**, 2345048 (2018).
[27] I. G. Richardson, Cem. Concr. Res. **34**,1733 (2004).
[28] M. J. A. Qomi, M. Bauchy, and R. J.-M. Pellenq, *Nanoscale Composition-Texture-Property Relation in Calcium-Silicate-Hydrates*, edited by W. Andreoni, and S. Yip (Springer International Publishing, Cham, 2020), pp. 1761.
[29] A. C. T. Van Duin, S. Dasgupta, F. Lorant, and W. A. Goddard, J. Phys. Chem. A **105**,9396 (2001).
[30] C. M. A, W. K. B, and K. B. A, Comput. Phys. Commun. **147**,222 (2002).
[31] A. van Duin, A. Strachan, S. Stewman, Q. Zhang, X. Xu, and W. Goddard, J. Phys. Chem. A **107**,3803 (2003).
[32] M. C. Pitman, and A. C. T. V. Duin, J. Am. Chem. Soc. **134**,3042 (2012).
[33] E. Demiralp, T. Çagˇin, and W. A. Goddard, Phys. Rev. Lett. **82**,1708 (1999).
[34] S. Plimpton, J. Comput. Phys. **117**,1 (1995).
[35] C. Zhao, W. Zhou, Q. Zhou, Z. Wang, G. Sant, L. Guo, and M. Bauchy, J. Colloid Interface Sci. **590**,199 (2021).
[36] I. G. Richardson, and G. W. Groves, J. Mater. Sci. **28**,265 (1993).
[37] A. S. Côté, A. N. Cormack, and A. Tilocca, J Phys Chem B **120**,11773 (2016).
[38] L. Martinez, R. Andrade, E. G. Birgin, and J. M. Martinez, J. Comput. Chem. **30**,2157 (2009).
[39] S. Nosé, Mol. Phys. **52**,255 (1984).
[40] W. G. Hoover, Phys. Rev. A **31**,1695 (1985).
[41] A. P. Horsfield, D. R. Bowler, H. Ness, C. G. Sánchez, T. N. Todorov, and A. J. Fisher, Rep. Prog. Phys. **69**,1195 (2006).
[42] S. G. E. Giap, J. Phys. Sci. **21**,29 (2010).

[43] S. Lin, C. Ionescu, K. J. Pike, M. E. Smith, and J. R. Jones, J. Mater. Chem. **19**,1276 (2009).
[44] E. L'Hopital, B. Lothenbach, G. Le Saout, D. Kulik, and K. Scrivener, Cem. Concr. Res. **75**,91 (2015).
[45] G. Renaudin, J. Russias, F. Leroux, C. Cau-dit-Coumes, and F. Frizon, J. Solid. State. Chem. **182**,3320 (2009).
[46] J. H. Kwak, J. Hu, D. Mei, C.-W. Yi, D. H. Kim, C. H. F. Peden, L. F. Allard, and J. Szanyi, Science **325**,1670 (2009).
[47] D. Coster, A. L. Blumenfeld, and J. J. Fripiat, J. Phys. Chem. **98**,6201 (1994).
[48] M. Ravi, V. L. Sushkevich, and J. A. van Bokhoven, J. Phys. Chem. C **123**,15139 (2019).
[49] G. A. Pozarnsky, and A. V. McCormick, J. Non Cryst. Solids. **190**,212 (1995).
[50] Y. Narendar, and G. L. Messing, Catal. Today. **35**,247 (1997).
[51] Z.-j. Wang, and I. Sohn, J. Am. Ceram. Soc. **101**,4285 (2018).
[52] E. Antoni, L. Montagne, S. Daviero, G. Palavit, J.-L. Bernard, A. Wattiaux, and H. Vezin, J. Non Cryst. Solids. **345-346**,66 (2004).
[53] J. M. Delaye, A. L. Gac, S. Macaluso, F. Angeli, F. Lodesani, T. Charpentier, and S. Peuget, J. Non Cryst. Solids. **567**,120936 (2021).
[54] P. Faucon, A. Delagrave, C. Richet, J. M. Marchand, and H. Zanni, J. Phys. Chem. B **103**,7796 (1999).
[55] E. M. Valliant, C. A. Turdean-Ionescu, J. V. Hanna, M. E. Smith, and J. R. Jones, J. Mater. Chem. **22**,1613 (2012).